Investigation on a Novel Injector Concept for Spinning Combustion Technology in High-pressure Conditions by advanced laser-based diagnostics

Andrei-Silviu MILEA[1,*], Aurélien PERRIER[1], Marcos CACERES[1], Alexis VANDEL[1], Gilles GODARD[1], Patrick DUCHAINE[2], Stéphane RICHARD[2], Gilles CABOT[1], Frédéric GRISCH[1]
1: Normandie Univ., UNIROUEN, INSA Rouen, CNRS, CORIA, 76000 Rouen, France
2: Safran Helicopter Engines, 64511 Bordes, France
* Correspondent author: frederic.grisch@coria.fr

Keywords: Spinning Combustion Technology; high-pressure combustion; PIV; OH-PLIF; NO-PLIF; kerosene-PLIF; NO pollutant;

ABSTRACT

Safran Helicopter Engines has recently patented the spinning combustion technology in which the burnt gases from one injector travel tangentially along the combustor annulus towards the neighboring injectors. Compared to conventional designs, the new kerosene injection systems are dedicated to improve air/fuel mixture ignition but also to further reduce NOx and soot particle emissions. Experimental studies are performed on these fuel injectors in a high-pressure/high-temperature combustion facility designed by the CORIA research laboratory. This test bench is able to reproduce the same operating conditions encountered in a helicopter combustor over the entire range of nominal operating conditions and has large optical accesses for the implementation of laser-based diagnostics. In the current paper, we present results concerning flame structure and NO formation in the primary zone under pressure conditions of up to 14 bar, using simultaneous OH-PLIF, NO-PLIF and kerosene-PLIF laser diagnostics. These experimental studies were supplemented by high-speed PIV measurements. A good spatial correlation between the distribution of liquid and vapour kerosene and the location of the flame front was observed. Depending on the operating conditions in terms of fuel/air ratio, mass flow rates and pressure, different flame structures resulting from the modification of the interaction between fuel injection and aerodynamics are observed. Furthermore, it was found that the Zeldovich pathway mainly controls the formation of NO in the vicinity of the flame front. In addition, the effects of FAR and pressure also have a significant impact on NO production. All these results are now intended to serve as a comprehensive validation database for the development and testing of high-fidelity LES tools dedicated to the simulation of reactive flows in aero-engine combustion chambers.

1. Introduction

Pollution is nowadays one of the biggest challenges addressed by the scientific community [1, 2]. Within this context, a significant increase in air traffic values are raising concerns towards the aeronautical manufacturers. Thus, more stringent regulations are implemented for the aircraft transportation while newer limits are proposed for the helicopter engines. In order to comply to the new tendencies and create more efficient and eco-friendly propulsion solutions for helicopters, Safran Helicopter Engines (SHE) developed the Spinning Combustion Technology (SCT) for the new generation of engines [3]. In a combustion chamber designed using this technology, a motion of revolution is produced inside the combustion chamber based on SCT. Thus, a helicoidal path is described towards the inlet of the turbine blades where the airflow enters without any additional deflection. As a result, a simpler design is considered for the combustor, which reduces the complexity and enhances the robustness of the engine. One of the main advantages of this technology is the net reduction of CO_2 by 15% with respect to the older engines. Moreover, the spinning motion of the reactive flow allows an improved ignition performance, a better flame stability, and a more homogeneous

temperature distribution at the inlet of the turbine. Today, this technology is evolving to reduce NOx and soot particle emissions. To achieve this, careful consideration is given to the liquid fuel injection system to improve fuel atomization, fuel/air mixing and combustion performance. To this end, the European LOOPS research program was initiated to support SHE in the development of these new injection systems, with the cooperation of two French research laboratories, CORIA for the experimental studies and CERFACS for the numerical CFD analyses, and the French industrial partner GDTech.

2. Objectives

Novel fuel-injection systems for SCT were studied experimentally to measure and quantify the NO and soot production by numerous advanced laser-based diagnostics in a high-pressure/high-temperature environment of fuel-rich combustion delivering intense chemiluminescence light. This paper addresses the experimental results and analysis of the NO production and aerodynamic field respectively for one of the injection systems fed with liquid kerosene. The velocity fields were measured both in non-reactive and reactive conditions by high-speed PIV whereas a dynamic study was performed in order to study the flame stability. Furthermore, the NO emission was analysed using the Planar Laser induced Fluorescence diagnostic. Furthermore, this diagnostic was combined with the PLIF-OH and PLIF-kerosene laser diagnostics to get a detailed understanding of the NO formation mechanism and also evaluate the evolution of this pollutant with respect to the flame structure and fuel spatial distribution.

3. Methodology

3.1 Combustion test rig

The HERON combustion test bench (Fig. 1) is designed to study house real-scale fuel nozzles for gas turbine engines without major modifications of their architecture [4, 5]. This enables a consistent assessment of the near-complete performance of fuel systems on an industrial scale. In addition, the architecture of this test rig is very similar to that of a single-injector tubular combustor, or a simplified cross-section of a traditional gas turbine annular combustor (Fig. 2). Therefore, studies performed in this combustion test rig are particularly representative of the global performance of the industrial liquid fuel nozzle inside the real engine.

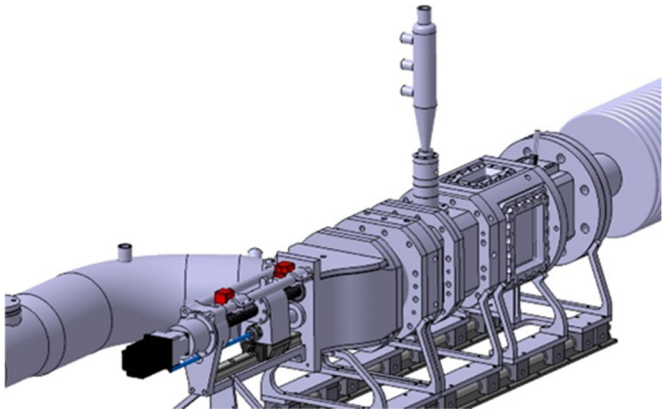

Fig. 1 HERON combustion test bench.

Furthermore, HERON is designed to reproduce the thermodynamic and mass-flow conditions specific to the operating conditions of a wide variety of aero-engines. Thus, the test bench reproduces the full range of nominal operating conditions of a helicopter powertrain combustor, and around 2/3 of the range of nominal points for a medium-sized aircraft jet engine. Hence, the experimental measurements performed in this test rig are of great importance for the manufacturers and the scientific community. In order to guarantee these operating conditions, HERON is able to sustain pressures up to 20 bar for high-temperature aeronautical reactive flows thanks to water cooling and air-film cooled optical windows. The test rig is delivering a maximum air mass flowrate of 300 g/s at 20 bar and a 10 g/s of liquid fuel. Air is supplied by a two-stage air compressor. The fuel used is the Jet-A1 aeronautical kerosene. Furthermore, an electrical heater raises the air inlet temperature up to 900 K in order to reproduce real conditions of a gas turbine engine combustor.

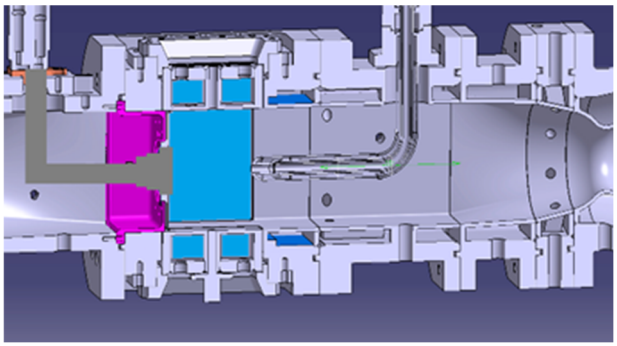

Fig. 2 Cut-section of the combustor.

HERON is composed by several modules: the injection module containing the fuel injector, the optical module with large optical windows to enable the study of the combustion primary zone and fuel atomization by non-intrusive advanced laser-based diagnostics, the dilution module designed to replicate the Quick-Quench for RQL injector designs, the secondary dilution module to further dilute and cool the exhaust gases and to ensure the oxidation and completion of any chemical evolution, and the exhaust module designed with a sonic nozzle to control the pressure condition inside the rig. One of a great advantage of the HERON combustion rig is the optical accessibility. The rig is equipped with two lateral 100x80mm UV quartz optical windows covering the entire height of the primary zone, and two 80x30mm optical windows located on the top and on the bottom of the module to allow the passage of the laser sheet inside the reactive flow (Fig. 2). The operating points presented in the current paper are displayed in Table 1.

Description (units)	Point 1	Point 2
Pressure (bar)	8	14
Inlet Air Temperature (K)	570	670
Fuel-Air-Ratio FAR (-)	68	41
Injector air mass-flow (g/s)	79.2	144.1
Jet A-1 fuel mass-flow (g/s)	5.39	5.9
Dilution air mass-flow (g/s)	100	12

Table 1: Operating conditions

Various laser-based diagnostics are used to measure the chemical and physical parameters of the reactive flow produced by the SCT injector. Hence, a series of challenges need to be addressed: high-pressure / high-temperature conditions, high-intensity light emitted by the fuel-rich flame, windows degradation from the flame, large liquid kerosene mass flow rates, and interference of the measurement signals with flame chemiluminescence. A combination of advanced filtering and post-processing techniques are applied to ensure the high-quality and fidelity of the results.

3.2 Aerodynamic field measurement

The high-speed Particle Image Velocimetry (PIV) laser diagnostic was developed in order to measure the 2D velocity spatial distribution in the primary zone downstream from the fuel injector outlet [6]. The assessment is performed both in combustion environment but also in a non-reactive heated airflow without liquid kerosene. A high-frequency acquisition rate of 10 kHz is tailored to capture the temporal evolution of the flow with high resolution. Hence, a double head Quantronix Dual Darwin Nd:YAG laser produces two laser pulses at 10 kHz. The output is set to 527nm with a power of around 22 W. The beams are converted into 60 mm laser sheets to perform 2D planar measurements. To this extent, a combination of two cylindrical lenses is used to form the parallel laser sheet, a cylindrical lens of focal f = -40mm converts the beam into a wide sheet, subsequently while a cylindrical lens of focal f = 450mm creates the parallel collimated laser sheet (Fig. 3). Furthermore, a spherical lens of focal f = 1500mm is located on the optical path to further focus the laser sheet into the flame. As the laser system is located far from the combustion chamber, a series of prisms is used to send the laser beam into the combustion chamber. ZrO_2 particles with a diameter of approx. 2.5 µm are seeded in the reactive flow due to their temperature resistance. The acquisition of the displacement of the seeding particles is performed by a Phantom V2512 high-speed camera. Therefore, it is used to capture series of two images at 10 kHz (i.e. 20kHz global acquisition rate). It is coupled with a Milvus Zeiss 2/100M optical objective (f = 100mm, f/2.8) together with a combination of optical filters (527nm interferential filter FWHM=10nm + 500-540nm band-pass filter) to collect efficiently the Mie scattered light.

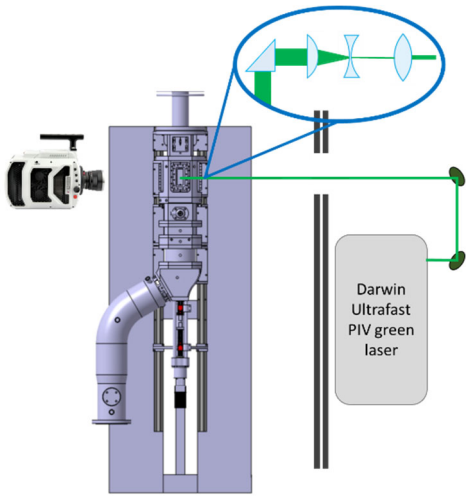

Fig. 3 Optical setup for PIV measurements

3.3 Coupled NO, OH and kerosene measurements

In order to assess the NO production, the NO-PLIF (Planar Laser-Induced Fluorescence) laser diagnostic is used in combination with the OH-PLIF and kerosene-PLIF diagnostics [7]. Thus, a coupled and correlated analysis can be performed for relevant operating conditions. A Precision Scan dye laser pumped by an Nd:YAG Quanta Ray Pro Series is used to create a laser beam at 226nm to excite the NO molecule. The pumping is performed at 532nm in a dye solution of Rhodamine 640, Rhodamine B and ethanol. The resulted 640 nm beam is mixed inside a BBO crystal with a 355nm laser beam issued from the pump laser system to get the 226nm. This UV wavelength allows an excitation of the $Q_1(29.5)$ rotational transition which delivers significant fluorescence signals at high temperatures Similarly, a second Sirah Precision Scan dye laser is used to excite both OH and kerosene at 282.75nm. To this extent, the pumping is undergone by an Nd:YAG Spectra Physics Quanta-Ray Pro Series at 532nm into a dye solution of Rhodamine 590 and ethanol. The UV output allows the excitation of the $Q_1(5)$ rotational transition for OH, whereas the mono and di-aromatic components of kerosene are excited together at the same wavelength. The detection of the OH radicals enables the location of reactive and burnt gases zones, while the kerosene detection highlights the region in which the fuel is atomized and evaporated. To ensure a simultaneous assessment of the OH, NO and kerosene without any interference between the signals, a 100ns time delay is imposed between both laser pulses. The output UV laser beams are both converted to thin laser sheets in order to perform measurements over a 2D plane crossing the center of the fuel injector. The optical arrangement to control the orientations of the laser beams is similar to the PIV experiments since the two Sirah Precision Scan laser systems are also placed remotely from the combustion chamber. A configuration featuring two cylindrical lenses (similar to the arrangement selected for PIV measurements) is implemented. Only the spherical lens is changed for a longer focal length (f=2500mm) to optimize the focal point inside the combustion chamber. The acquisition of the fluorescence signals is performed by four intensified emICCD cameras (Fig. 4).

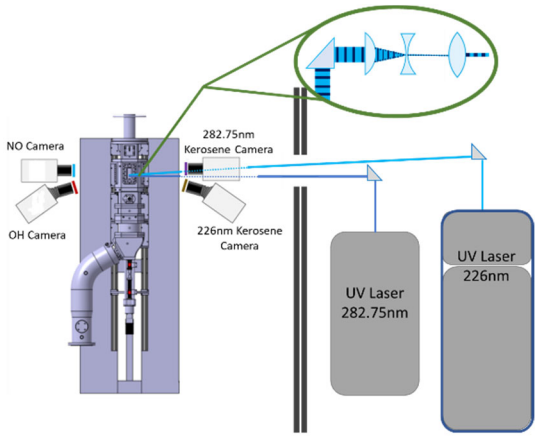

Fig. 4 Optical setup for combined measurements

Since the collected signals are mainly in the UV range, all the cameras are equipped with CERCO UV 100 mm f/ 2.8 objectives. Different Optical filters are used depending on the species detected: an interferential 310nm FWHM = 10nm filter is used for the OH radical, a short pass 276nm filter cutting until 1200nm for the NO fluorescence signal, a 250-400nm combined with a long pass 305nm for the kerosene fluorescence excited at 282.75 nm and a 315-400nm filter for the kerosene fluorescence issued from the 226nm laser beam excitation. The latter images are mainly used to correct light interference induced by kerosene fluorescence on the NO fluorescence images.

4. Results

4.1 Aerodynamic results

The non-reactive airflow at 8 bar from Fig. 5-left displays a large non-symmetrical behavior. In the outer recirculation zone, the vortices are defined similarly while the inner recirculation vortices are noticeably shifted. Overall, the topology under non-reactive conditions can be compared to a conventional stratified vortex flow, with the exception of the inward offset of the recirculation zones and a curved upper injection.

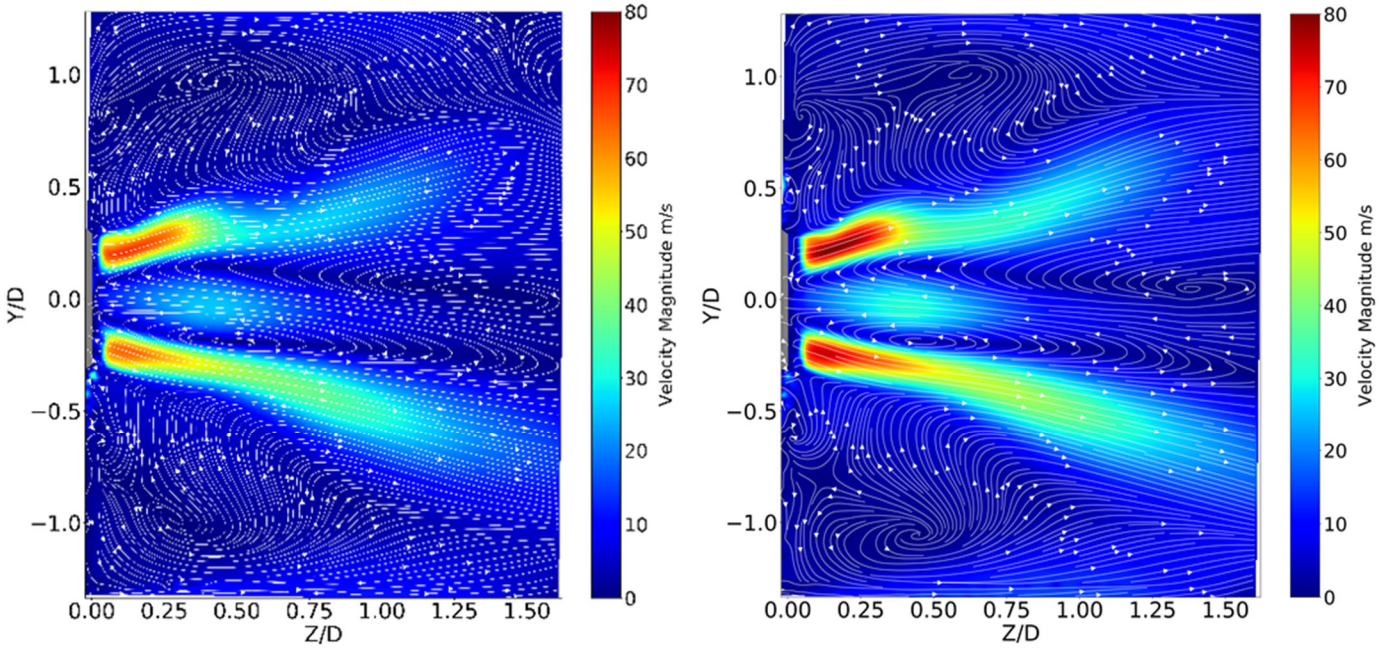

Fig. 5 Non-reactive aerodynamic fields for 8 bar 570K (left side), 14 bar 670K (right side).

In addition, Fig. 5-left shows greater flow acceleration in the lower Y/D section, with an accentuated mean velocity range extending towards the dilution zone. However, the velocity range in the upper part of the Y/D zone shows higher velocities over a smaller area. A deceleration zone can be noted downstream of the injector in the upper high-speed zone, mainly produced by an air stream coming from the cooling slots. This presence of air disrupts the symmetry of the flow, since in the lower Y/D zone, the cooling air merges with the high-speed injection zone, following the trajectory of the main injected air flow. A curvature specific to the injector geometry produces a different kinetic energy at the injector outlet between the two acceleration zones shown in the 2D image. The non-symmetrical behavior of the high

and medium velocity zones is consistent with the difference between the internal recirculation zones. It is important to note that 3D effects also play an essential role in the development of the injector outlet flow. The barking effect in the positive Y/D region could in fact be driven by a larger transverse vortex. Downstream in the far field, the flow continues to develop towards the dilution module in the lower heights (Y/D-) while an additional recirculation zone is observed in the upper zone (Y/D+). This structure favors the penetration of the cooling air in the far field. As a result, the region starting at Z/D = 1 appears to be pushed downwards. This effect can be observed on the slightly downward-shifted inner recirculation in Fig. 5-left.

Figures 5-left and 5-right are very similar, despite the different operating conditions. However, significantly higher velocities are observed at the injector outlet at 14 bar (Fig. 5-right), due to a higher air mass flow rate. Consequently, the central recirculation zone is characterized by the presence of higher velocities at higher pressure. On the other hand, the outer recirculation zones exhibit more pronounced vortices that move axially downstream as the entire flow is pushed due to the higher mass flow rate and hence higher axial velocities. The 14 bar condition (Fig. 5-right) shows symmetrical far-field behavior at the ends, unlike the 8-bar condition. A greater axial offset between the outer recirculation zones prevents the formation of an additional vortex downstream in the positive Y/D zone. If we disregard the curvature of the upper mean velocity band (Z/D = 0.6, Y/D = 0.5) possibly caused by a 3D structure, the overall shapes of the injection velocity distribution are similar.

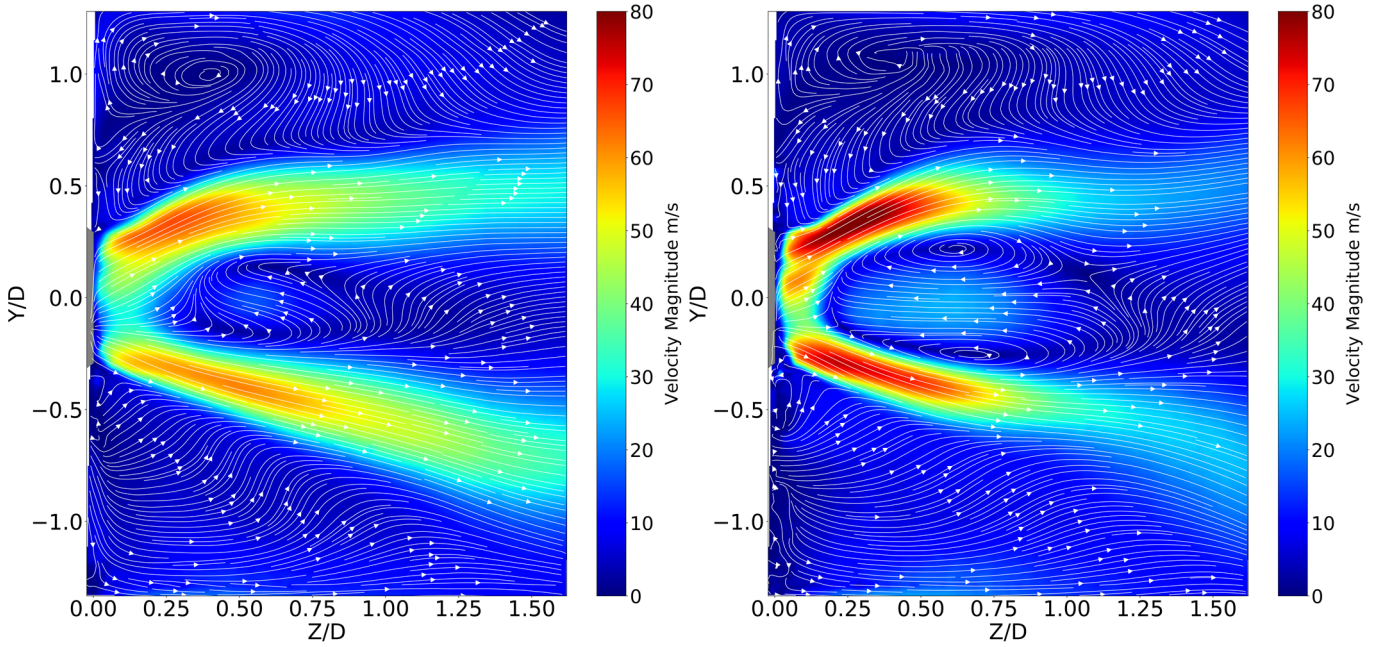

Fig. 6 Reactive flow aerodynamic fields for 8 bar 570K (left side), 14 bar 670K (right side).

With respect to the reactive flow, it is essential to note the difference with respect to the non-reactive conditions. Both pressure conditions present an acceleration of the flow locally due to the higher temperatures representing higher-energy levels. First of all, at 8 bar (Fig. 6-left), the recirculation zones are significantly changed. In the outer area, only the superior (Y/D +) recirculation zone is shaped. This flow pushes downward the superior high-velocity range. The

negative Y/D outer zone is characterized by the strong axial displacement of the cooling air without recirculation. On the other hand, the inner recirculation is not fully defined because of the central axial airflow of high velocity pushing the vortices downstream. Since the upper injection band is entirely pushed inwards by the outer recirculation, the distance between the injection branches decreases in the measured plane. Thus, the circular flow is unable to fully develop in the center. As a result, in the lower part the beginning of the circular movement is well shaped. However, the inertia of the high-velocity superior injection drags along the flow and prevents the closure of the recirculation. Furthermore, during combustion (Fig. 6-left) the discrepancy between the injection zones is accentuated since the superior part (Y/D +) highlights a wider more concentrated high-velocity area compared to the lower part (Y/D -). This difference also impacts the formation of the inner recirculation. Furthermore, in the far field the outer area of the flow is pushing inwards towards the center, meaning a 3D wider structure is present in that area. Second of all, the higher pressure of 14 bar (Fig. 6-right) displays a completely new behavior. The velocity field presents a great resemblance with a swirled stratified combustion, namely in the central area. The inner recirculation zone is well defined with two symmetrical opposite eddies. This can be explained by the higher pressure preventing the airflow to strongly develop axially. Thus, the injection branches open widely and the eddies expand entirely. However, the outer recirculation zone is similar to the 8 bar condition: an enhanced superior (Y/D +) recirculation zone pushing towards the center, and an strongly axial displacement in the inferior zone (Y/D negative). The injection velocity distributions are non-symmetric and similar to 8 bar condition except the diminished length of the high-velocity regions (Fig. 6-right). This is due to the increase in pressure that shortens the axial development. 3D effects are enhanced at high pressure and impact especially the outer flow.

4.2 Flame topology, fuel and NO distributions

The combined measurements of instantaneous kerosene fuel, OH-PLIF and NO-PLIF distributions were recorded to examine the mechanisms of NO formation and transportation inside the combustion chamber. In addition, the velocity distributions, measured separately by PIV, were used to provide indications of the interplay between the aerodynamical flow and the chemical processes at the injector outlet. Experiments were performed for two conditions of pressure, 8 and 14 bar. Figure 7 displays typical instantaneous distributions of kerosene, OH and NO for a pressure of 8 bar. In terms of kerosene fuel distribution, a hollow cone injection is observed. The grey area in the kerosene image indicates the presence of liquid kerosene, while the dark area between the grey area and the white contour line represents the vapor-phase fuel region. It should also be noted that the grey areas, which are experimentally detected with a low spatial resolution, indicate the presence of a condensed mixture of liquid ligaments and fuel droplets at the injector outlet. The spatial distribution of kerosene shows a large quantity of liquid in the upper part of the flow, where it is distributed over a maximum axial distance of Z/D=1.0. This effect is the consequence of its high velocity transportation (see PIV results) after leaving the injector. In contrast to the upper part of the flow, a smaller quantity of kerosene is detected in the lower part of the flow, suggesting that the kerosene distribution exhibits an asymmetric pattern on leaving the injector. This effect is real and cannot be explained by measurement artefacts such as a misalignment of

the laser sheet in respect of the kerosene injection holes or by any partial absorption of the laser sheet's energy along the kerosene flow. Indeed, the alignment of the laser sheet along the center of the upper and lower kerosene injection holes was carefully checked during the experiments. In addition, the absorption coefficient of liquid kerosene at the 282 nm wavelength is too low to explain such a reduction in signal intensity between the upper and lower parts of the flow. This effect is undoubtedly due to the geometry of the liquid kerosene distributions with the swirling air flow in this injector, which modifies the good homogenization of the fuel-air mixture and thus favor the upper part of the flow in terms of the quantity of liquid fuel injected.

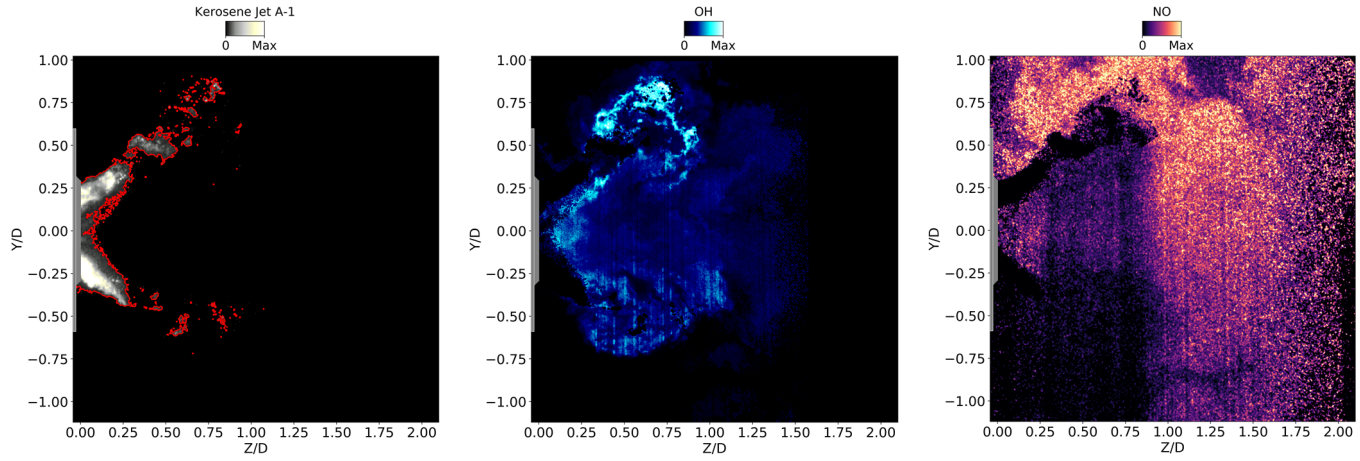

(a) (b) (c)

Fig. 7 Instantaneous kerosene-PLIF (a), OH-PLIF (b) and NO-PLIF (c) distributions at the injector outlet for Point 1.

The instantaneous distribution of OH (blue colors in Fig. 7b) confirms that in the lower part of the flow, a reaction zone is located on the inner part of the kerosene region and that no combustion occurs on the outer part. On the contrary, in the upper part of the flow, combustion occurs mainly at the outer boundary and at the end of the jet of kerosene. Once OH was produced, this one is transported downstream of the combustion chamber as long as the temperature of the flow remains high. Due to the re-entry of hot gases along the flow axis, pockets of OH from the exhaust gases are also observed in the core of the flow. In addition, the analysis of instantaneous OH-PLIF images (see figure 7b) reveals a more intense reaction zone in the positive Y/D zone. The difference in intensity between the upper and lower areas of the measured plane confirms the presence of a larger reaction zone in the positive Y/D reaction zone. This difference in intensity between the upper and lower zones confirms the existence of a non-symmetrical flow, as has already been observed with the velocity and kerosene distributions.

As the 226 nm laser sheet undergoes a strong attenuation of intensity during its transport through the flow and in particular after crossing the kerosene region (high absorption coefficient of kerosene), no NO fluorescence could be detected in the central zone of the flow located close to the kerosene zone (see Fig. 7c). For this reason, only the spatial distributions of NO on the upper side of the flow were examined. Maximum NO fluorescence is produced in the upper

reaction zone (presence of a thin region at the periphery of the boundary between the kerosene and OH distributions) which indicate a preferential production of NO at high temperatures by the Zeldovich thermal mechanism [8].

Although velocity measurements could not be performed in the region close to the injector outlet (Z/D<0.1), due to the presence of intense stray light caused by the laser sheet on the injector wall, a comparison of the mean velocity distribution in the upper part of the flow and in the region at Z/D<0.2 with the mean kerosene distribution shows that the mean velocity of the flow is greatly reduced compared with the maximum velocity observed in the flow, and that the streamlines are oriented at the outlet of the injector with a slight inclination, as is the orientation of the kerosene distribution (Fig. 8a). After Z/D=0.2, the velocity streamlines along the flow axis are deflected towards the upper part of the flow due to the existence of an intense recirculation zone centered on the flow axis, preventing any significant axial transport of the flow. Similarly, the flow at the outer periphery of the kerosene jet is itself deflected and strongly accelerated due to the development of a flame front, with a high temperature gradient leading to an increase in velocity (see OH fluorescence image). The jet of kerosene is then transported between the two zones, causing the deviation observed. Beyond Z/D=0.2, the kerosene distribution spreads progressively radially due to intense evaporation resulting from the increase in temperature. Kerosene consumption by combustion occurs at an axial distance of Z/D=0.3-0.4. It should also be noted that the presence of a large internal recirculation zone along the flow axis favors the re-injection of hot gases into this region. This effect promotes the rapid removal of kerosene at a distance Z/D of less than 0.1 along the flow axis, while allowing the flame to be stabilized efficiently. In the lower part of the flow, the jet of kerosene is transported and distributed radially in an orientation similar to the streamlines observed experimentally. In contrast to the area above the flow axis, kerosene is mainly consumed at the inner boundary of the fuel jet and at the end of the fuel zone (see figure 8a). Similarly, no combustion is observed along the outer boundary of the kerosene jet.

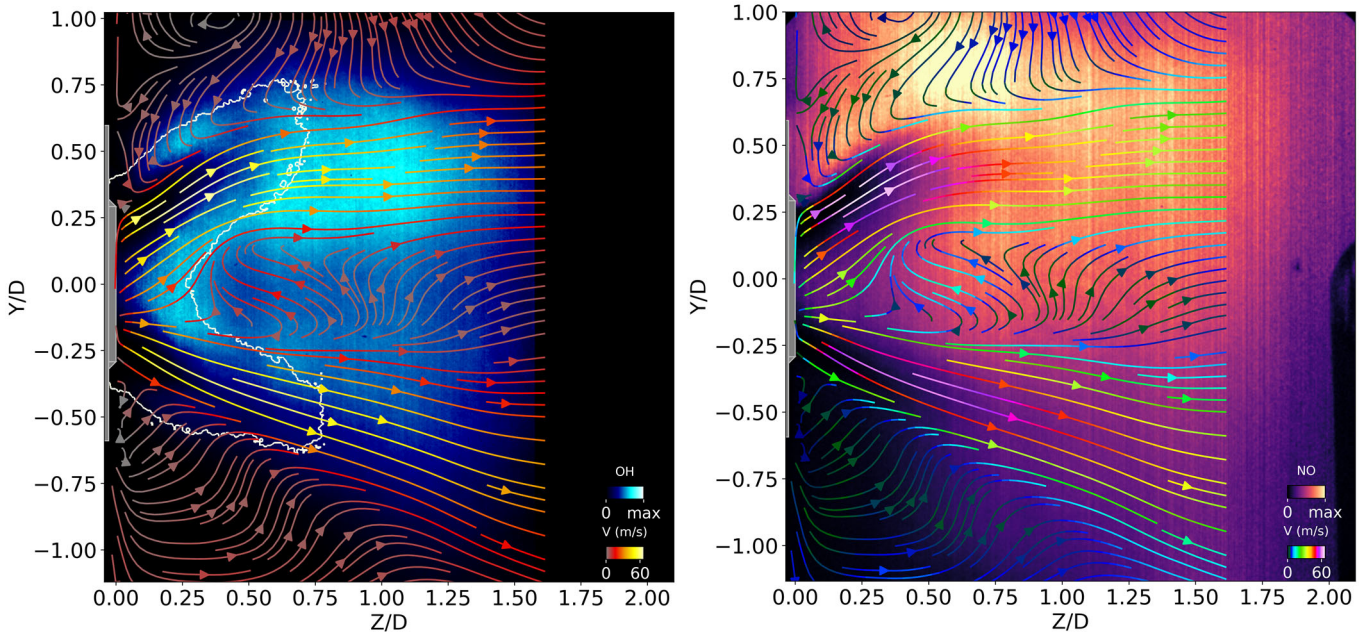

Fig. 8 Point 1 condition - OH distribution with kerosene borders (left side), NO distribution (right side).

The areas of high NO concentration correspond to the same areas of high OH gradients observed in Figs 8a-b, i.e. near the flame front (higher temperature due to exothermic combustion). A NO intensity peak is also observed away from the OH zones (Z/D~0.6, Y/D=0.75). This pocket is located close to the external recirculation zone in which an air stream comes from the cooling slots. As the temperature is not elevated in this region, a first chemical transformation of air and exhaust gases in N_2O then in NO can be envisaged [8]. The decrease in NO intensity outside this reactive flow indicates a transportation of NO into the outer recirculation zone and deeper into the combustion chamber. It should also be noted that a few quantities of NO are observed in the center of the flow and may even penetrate along the core of the flow. This phenomenon can be further clarified by examining the 2D mean distributions of OH and NO (see Fig. 8). Indeed, the correlation of these mean spatial distributions with the velocity streamlines reveals that the largest and most intense pockets of NO in the upper zone of the flow are originally created along the flame front while continuing to be transported throughout the upper zone at high velocity (see Fig. 8b).

Figure 9 displays typical instantaneous distribution of kerosene, OH and NO distributions for a pressure of 14 bar. The spray pattern is almost symmetrical, with a slightly larger upper branch (Figure 9a). Combustion takes place around the fuel jet, which comes closer to the injector outlet section along the flow axis. The measurements show a flame topology similar to that of conventional aeronautical swirl injectors operating under lean conditions, such as multipoint injectors [8]. Stabilization in the inner zone of the injection dome is favored by the fully developed recirculation zones. As the kerosene distribution is quasi-symmetrical, a symmetrical V-shaped reactive flow is observed, unlike the flame observed at 8 bar (Figure 9b). A substantial increase in the opening of the kerosene jet and subsequently in the flame region occurs as a result of the increase in pressure in the combustion chamber. Figure 9c shows the spatial distribution of the NO pollutant at a pressure of 14 bar. It can be observed a better observation of NO by PLIF close to the central zone of the injector, these ones being the consequence of the fast consumption and kerosene after leaving the injector. As observed at 8 bar, NO is first produced near the front flame and then are convected into the combustion chamber according to the preferential flow orientations

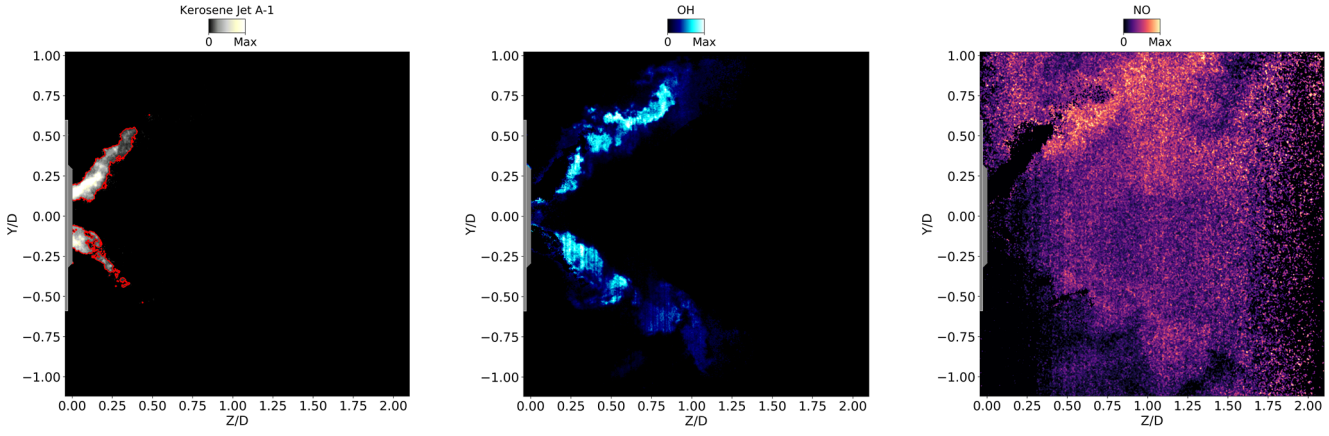

(a) (b) (c)

Fig. 9 Instantaneous kerosene-PLIF (a), OH-PLIF (b) and NO-PLIF (c) distributions at the injector outlet for Point 2.

Figure 10 displays the mean-distributions of OH, kerosene and NO together with the velocity streamlines for the point 2 condition. As already observed on the instantaneous PLIF images shown in Fig. 9, the mean flame is a V-shaped symmetrical flame resulting from a better spatial distribution of kerosene at the injector outlet (Fig. 10a). An observation of Fig. 10b showing the average spatial distribution of the NO pollutant shows that NO production is lower than in the rich conditions of 8 bar (same scales for the two images). It can be noted that at the highest pressure, the regions of maximum NO production are observed in the immediate vicinity, and are even superimposed on the strong OH gradients also representing the combustion zones (Fig. 10a). The thermal mechanism of NO production is therefore predominant in this region. Although lean mixing conditions at high pressure are theoretically favorable to the nitrous oxide mechanism, the dominant factor in NO formation remains the high temperature. The lower NO values at 14 bar result from the leaner mixing that prevents local stoichiometric pockets at high temperature, unlike at 8 bar. At 14 bar, a significant amount of NO is also found along the flow axis due to the transportation of NO towards the internal recirculation vortices that trap this pollutant.

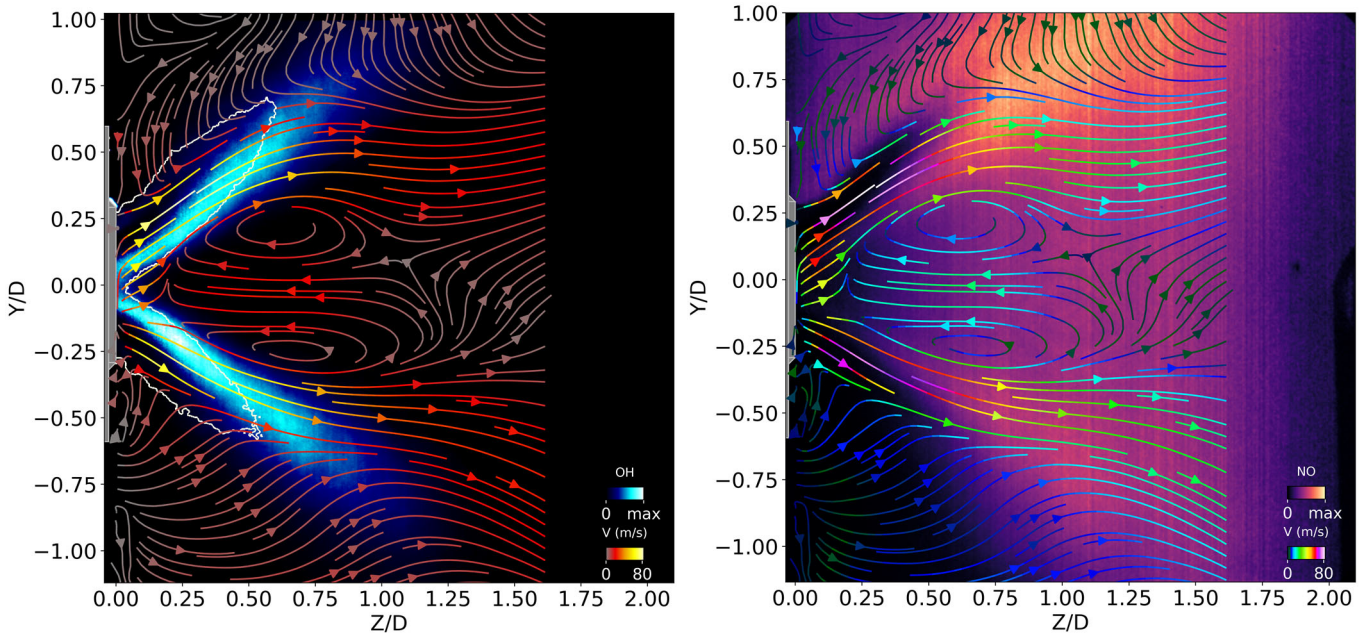

Fig. 10 Point 2 condition - OH distribution with kerosene borders (left side), NO distribution (right side).

5. Conclusion

Advanced laser-based diagnostics are implemented with success in a high-pressure/high-temperature test facility for different operating points: 8bar 570K FAR68 and 14 bar 670K FAR41. The aim of the current study was to determine with accuracy the performance of novel concepts of kerosene injector for the spinning combustion with a focus on the NO production. The aerodynamic field is studied via the PIV laser diagnostic at non-reactive and reactive conditions. A noticeable change in the velocity field is observed during combustion with respect to the non-reactive condition. Similar behavior is highlighted at non-reactive conditions. In combustion, at 8 bar, a non-symmetrical behavior is observed while a more traditional aerodynamic structure is noticed at 14 bar. A simultaneously coupled OH-PLIF, NO-

PLIF and kerosene-PLIF campaign was initiated to assess the NO production and analyze the flame topology. A non-symmetrical bulkier reactive area is distinguished at 8 bar even though the fuel spatial distribution is quasi-symmetric. On the other hand, the 14 bar pressure condition highlights a V-shape flame similar to conventional lean aeronautical flames produced by multi-point fuel injection systems. A thin reactive region located inside the kerosene spray is observed at 14 bar whereas a bulkier compact reactive region located on the upper part is distinguished at 8 bar. In terms of NO, the 8 bar pressure condition appears to be more favorable to the NO production because of the relatively close FAR to the stoichiometric represented by high temperatures. Moreover, the aerodynamic particularities of the flow at 8 bar bring into discussion other NO formation mechanism. On the other hand, at 14 bar, main of the NO production is governed by the temperature. The outer boundaries of the kerosene spray, where combustion oxidation takes place, represent the zones of NO production, while the central zone is loaded with NO due to its convection by the flow. Lowering the FAR appears to be a promising solution for reducing the concentration of this pollutant.

Acknowledgements

This project has received funding from the Clean Sky 2 Joint Undertaking (JU) under grant agreement No 882300. The JU receives support from the European Union's Horizon 2020 research and innovation programme and the Clean Sky 2 JU members other than the Union.

References

[1] Chapter 4 - Air and water pollution: An important nexus of transportation and health, Editors: M.D. Meyer, O.A. Elrahman, Transportation and Public Health, Pages 65-106, Elsevier, 2019

[2] ICAO, Trends in Emissions that affect Climate Change, 2016

[3] N. Savary, G. Taliercio, The Safran helicopter engine spinning flame combustor concept to meet customer needs, 42nd European Rotorcraft Forum September 5–8, 2016

[4] F. Grisch, A. Boukhalfa, G. Cabot, B. Renou, A. Vandel, CORIA Aeronautical Combustion Facilities and Associated Optical Diagnostics, AerospaceLab Journal, Issue 11, 2016

[5] S. Legros, C. Brunet, P. Domingo-Alvarez, P. Malbois, E. Salaun, G. Godard, M. Caceres, B. Barviau, G. Cabot, B. Renou, G. Lartigue, V. Moureau, S. Puggelli, S. Richard, M.A. Boukhalfa, F. Grisch, Combustion for aircraft propulsion: Progress in advanced laser-based diagnostics on high-pressure kerosene/air flames produced with low-NOx fuel injection systems, Combustion and Flame, Volume 224, 2021

[6] I. Boxx, C.M. Arndt, C.D. Carter, W. Meier, High-speed laser diagnostics for the study of flame dynamics in a lean premixed gas turbine model combustorExp. Fluids 52 (3), 555-567

[7] Malbois P.; Salaun E.; Frindt F.; Cabot G.; Renou B., Grisch F., Bouheraoua, L., Verdier, H., Richard S., 2017 Experimental Investigation with Optical Diagnostics of a Lean-Premixed Aero-Engine Injection System Under Relevant Operating Conditions GT2017-64484, Proceeding of the ASME Turbo Expo, Charlotte – USA.

[8] Lieuwen T.C., Yang V., Gas Turbine Emissions, 2013, Cambridge University Press.

[9] Nicol, D. G., Steele, R. C., Marinov, N. M., Malte, P. C., 1995, The Importance of the Nitrous Oxide Pathway to NOx in Lean-Premixed Combustion, Journal of Engineering for Gas Turbines and Power 117 pp 100-112.